PAPER • OPEN ACCESS

Toward zero-excess lithium sulfur batteries: a systematic cell parameter study

To cite this article: Joshua H Cruddos *et al* 2025 *J. Phys. Energy* **7** 025006

Journal of Physics: Energy

PAPER

Toward zero-excess lithium sulfur batteries: a systematic cell parameter study

Joshua H Cruddos[1,2,4], James B Robinson[1,2,4], Paul R Shearing[3,4] and Alexander J E Rettie[1,2,4,*]

[1] Electrochemical Innovation Lab, Department of Chemical Engineering, University College London, London WC1E 6DH, United Kingdom
[2] Advanced Propulsion Lab, Marshgate, University College London, London E20 2AE, United Kingdom
[3] The ZERO Institute, University of Oxford, Holywell House, Osney Mead, Oxford OX2 0ES, United Kingdom
[4] The Faraday Institution Quad One, Harwell Science and Innovation Campus, Didcot OX11 0RA, United Kingdom
[*] Author to whom any correspondence should be addressed.

E-mail: a.rettie@ucl.ac.uk

Keywords: zero excess Li, anode free, Li sulfur, Li sulfide

Supplementary material for this article is available online

OPEN ACCESS

RECEIVED
24 October 2024

REVISED
30 December 2024

ACCEPTED FOR PUBLICATION
7 January 2025

PUBLISHED
22 January 2025

Abstract

Zero-excess lithium (ZEL) or 'anode-free' batteries aim to minimize negative electrode material and address the challenges associated with handling thin lithium metal foils during fabrication. To date, most studies in the field of ZEL cells have primarily focused on lithium-ion chemistry, with considerably fewer systematic investigations into ZEL-sulfur (ZELiS) cell fabrication and optimization. Here we develop a ZELiS battery, comprising a Li_2S-based composite positive electrode on carbon paper paired with a Ni foil current collector (CC) and evaluate the effects of various CC materials, electrolyte volume to Li_2S mass ratio and C-rate. The developed cells reproducibly achieve an average Coulombic efficiency of 99% from cycles 2 to 200, and a final capacity of 272 mAh $g^{-1}{}_{Li2S}$ at a C/10 rate. Furthermore, we employ x-ray computed tomography to elucidate the morphological changes and degradation processes occurring within the positive electrode composite, revealing the irreversible loss of Li_2S/S_8 during cycling, which is exacerbated at high rates. These results should be useful in the development of commercially viable ZEL energy storage devices.

1. Introduction

Energy storage devices with improved volumetric and gravimetric energy densities beyond Li-ion batteries are essential to mitigate the effects of climate change [1]. One promising candidate is lithium sulfide (Li_2S) as the active positive electrode component, due to its high theoretical capacity (1,167 mAh g^{-1}) as well as the relative abundance, low cost and favourable geographic distribution of its sulfur precursor [2, 3] compared to materials used in Li-ion positive electrodes. To achieve a commercially viable Li_2S battery, a loading $>$ 5 mg $cm^{-2}{}_{Li2S}$ would be required, equating to an energy density of greater than 500 Wh kg^{-1} [1]. Previous commercial studies into pouch-type Li-S cells only achieved 350 Wh kg^{-1} and 300 Wh kg^{-1}, both for less than 100 cycles [4, 5]. Whilst advances in this technology have been made, widespread commercialisation has been hampered by a range of challenges.

The insulating nature of sulfur and Li_2S necessitates the addition of a greater proportion of conductive additives than is required for Li-ion batteries. These typically comprise around 30 wt%, which in turn reduces the energy density of the cell [6, 7]. Significant research has been undertaken to increase the active material loading of Li-S cells [8], however high loading often results in poor electrochemical performance due to low sulfur utilisation and an increase in the polysulfide shuttle effect [9]. Furthermore, the electrochemical performance can be improved by the addition of an excessive mass of conductive carbon to the positive electrode composite and substrate [10, 11]. In some instances, as little as 20% sulfur loading is incorporated into the positive electrode, which results in a gravimetric capacity too low to be practical [12].

Additionally, most Li-S cell research is conducted using coin cells which use a Li metal foil as the negative electrode. Although convenient for small scale testing, this approach can equate to a negative-to-positive electrode ratio (N/P ratio) of over 50 [3, 6], where a value closer to 1 would be desirable. Li's low reduction potential (−3.04 V vs. the standard hydrogen electrode) causes irreversible loss of active S species during operation: as polysulfides shuttle over to the negative electrode they are irreversibly reduced to solid Li_2S resulting in a loss of active material and negative electrode surface area [13, 14]. Furthermore, there are manufacturing challenges involved with the large-scale use of thin Li metal foils, and self-discharge can occur as they are assembled in the charged state [15].

The dynamic nature of the Li metal electrode also poses challenges. When Li deposits it undergoes inhomogeneous nucleation resulting in a very high surface area solid electrolyte interphase (SEI). Side reactions continuously occur between Li-metal and the ether-based electrolyte leading to the consumption of both [16]. Electrolyte additives, such as $LiNO_3$, are routinely added due to their proficiency in stabilising the SEI and improving Li plating/stripping. However, this does increase the presence of none-active species in the cell [17]. Moreover, electrochemically 'dead' Li can be produced which dramatically reduces Li inventory [18]. To mitigate this effect in research laboratories, large excesses of both Li and liquid electrolyte are often used, however this is undesirable as it reduces energy density while increasing raw material costs. Sparingly solvating electrolytes are an attractive alternative, which help to mitigate polysulfide shuttling and subsequent active material reduction at the negative electrode. However, these can lead to poor material utilisation and insufficient wetting of the active lithium sulfide species [19, 20]. To realise high-energy-density Li-S batteries, cells with high active-sulfur-content, low electrolyte-to-sulfur ratios, and ultra-thin Li metal negative electrodes (N/P ratio < 5) are required [1, 21].

To minimise the use of excess Li within the cell, an alternative approach involves preparing the positive electrode in the discharged state (i.e. Li_2S) and pairing it with a bare metal current collector (CC) [9, 17]. Typically, Ni foil has been the preferred CC choice, however other studies have successfully implemented Cu and stainless steel [15]. Li is reversibly plated and stripped on/from the CC, resulting in an initial N/P ratio of no greater than 1. As all Li is initially contained in the Li_2S composite electrode, manufacturing challenges associated with thin Li metal foils are bypassed (although new ones stemming from Li_2S are noted) as is self-discharge. We term this configuration a zero-excess Li-S (ZELiS) cell, as opposed to 'anode-free' because: (i) anode is poor electrochemical terminology (only true during discharge for secondary cells) and (ii) while the Li negative electrode is not initially present, the cell always operates with positive and negative electrodes.

While many challenges are shared between LiS and ZELiS cells, e.g. Li metal electrode dynamics, continuous electrolyte consumption and the polysulfide shuttle effect, new issues also arise [21]. Since Li_2S is effectively both electronically and ionically insulating [22], the use of conductive agents is imperative, with a particular focus on using high surface area carbon to promote the initial oxidation-nucleation reaction of Li_2S [12]. To further improve the kinetics of this reaction, high energy ball milling is routinely employed to reduce the particle size. Even with these efforts, cells must be charged at high overpotentials ($>$3.0 V) in the formation cycle to activate Li_2S [23, 24]. In addition, the first 5 cycles tend to show poor Coulombic efficiency (CE), as low as 50%, leading to rapid capacity fade. As a result of the N/P ratio being effectively equal to 1, any degradation of the Li negative electrode results in excess S species, making performance closely dependent on the efficiency of reversible Li deposition onto the metallic CC [11, 25]. Overall, cell-wide improvements must be made to achieve commercial viability.

So far, studies conducted on similar cell configurations have primarily focused on attempting to improve SEI formation and reversible Li plating/stripping [10, 15, 18, 26, 27]. However, cell design and testing parameters used vary widely, making comparison difficult. Thus, a detailed investigation of robust 'benchmark' ZELiS cells is required to enable rational modifications and achieve the goals of minimising inactive material content (e.g. conductive additives and binders), low electrolyte volumes and high sulfur loading. Furthermore, the lack of excess Li and rapid capacity fade make it an attractive platform to quickly evaluate the efficacy of cell modifications.

Here, we present a ZELiS coin cell design which exhibits reproducible electrochemical cycling up to 200 cycles. After establishing a robust cell architecture and active material loading value, we systematically varied the CC material and electrolyte volume vs Li_2S loading ratio. Electrochemical testing was used to interrogate the formation process as well as long-term cycling of the optimised cell at various rates, while changes in Li_2S/S_8 particle morphology and distribution were visualised by x-ray micro-computed tomography. We conclude with recommendations and future directions towards commercially relevant ZELiS cells.

2. Methodology

2.1. Li_2S ink and positive electrode preparation

Lithium sulfide powder (Li_2S, Fisher Scientific) and conductive carbon additive (C-NERGY super C65, Timcal) were used as received and combined in a zirconia planetary ball milling jar, containing zirconia milling media (Retsch), in a ratio of 7:2, before being dry milled at 500 rpm in 10 min on/off intervals for 18 h in a planetary ball mill (PM 100, Retsch). 10 wt.% styrene co-butadiene (Sigma Aldrich) was pre-dissolved in toluene (anhydrous, Sigma Aldrich) and subsequently wet milled at 500 rpm in 5 min on/off intervals for 2 h.

The resulting slurry was drop-cast using a pipette (Research Plus, Eppendorf) onto pre-dried, pre-cut 14 mm diameter carbon paper substrates (AvCarb P50, Fuel Cell Store). These were allowed to dry under ambient glovebox conditions overnight, then dried again overnight at 80 °C under vacuum in a Buchi oven (B-585, Buchi).

2.2. Electrolyte preparation

All materials including electrolyte salts, molecular sieves (3 Å, Fisher Scientific), and PTFE syringe filter tips (0.2 μm, Fisher Scientific) were dried under vacuum at 120 °C, 220 °C and 80 °C respectively for three days. Under glovebox conditions (Ar atmosphere, $<$1 ppm O_2 and H_2O, MBraun), anhydrous solvents were used throughout and dried with the molecular sieves for an additional three days. The solvents were filtered through PTFE syringes into a dry pristine glass vial ready for use. 1 M bis(trifluoromethane)sulfonimide lithium salt (LiTFSI, Sigma Aldrich) and 0.8 M lithium nitrate ($LiNO_3$, Sigma Aldrich) were dissolved under stirring in a 1:1 vol/vol mixture of 1,3-dioxolane (DOL, dried, Sigma Aldrich) and 1,2-dimethoxyethane (dried, Sigma Aldrich) [28–30].

2.3. Materials characterisation

Powder XRD was performed on a SmartLab SE diffractometer (RIGAKU) using a 2 kW Cu source Kα1 and Kα2 ($\lambda = 1.541$ & 1.544 Å) operating in Bragg-Brentano mode. Scans were carried out in a 2θ range of 0°–60° with a step size of 0.01° and a speed of 1.0° min^{-1}. Samples were measured on a zero-background silicon wafer sample holder. Samples for scanning electron microscopy (SEM) were adhered to pin stubs (Agar Scientific) using double sided carbon tape (Fisher Scientific). The SEM images were taken in SE2 mode using an EVO-100 (ZEISS) at 15 kV and a working distance of 7 mm.

2.4. Electrochemical measurements and characterisation

Coin cells were prepared inside a glove box using CR2032-sized coin cell casings (Pi-Kem) containing Li_2S positive electrodes and 15 mm diameter Cu, Ni or stainless steel (Pi-Kem) foils as the CC negative electrode. Two 0.5 mm and one 0.2 mm thick steel spacers (Pi-Kem) were used alongside a 16 mm diameter Celgard 2400 separator. Electrolyte was pipetted onto the separator prior to the addition of the positive electrode. Cells were electrochemically tested at room temperature using a BioLogic cell cycler (BCS-805, BioLogic). A 4-point connection type holder (CCH-1, BioLogic) was used and cells were rested for 2 h prior to galvanostatic charge/discharge cycling between cut off voltages of 2.8 and 1.8 V [30]. Electrochemical impedance spectroscopy (EIS) measurements were conducted using a VMP-300 potentiostat (BioLogic) using a 10 mV perturbation voltage over a frequency range of 1 MHz to 0.1 Hz [31].

2.5. X-ray micro-tomography

Ex-situ micro-tomography was performed using a lab based micro-CT instrument (Xradia Versa 620, Zeiss). Once charged to the desired the state, the coin cells were transferred to an Ar-filled glovebox, de-crimped and the Li_2S positive electrodes removed from the casings. A 1 mm diameter sample was hole punched and positioned within a 1.5 mm diameter PEEK holder (Swagelok). Steel pillars with ferrules were inserted above and below the sample and tightened to ensure the holder was air-tight during measurements.

An optical magnification of 20$\times$ was used, and a bin size of 1 was applied to the 2048 $\times$ 2048 px CCD detector, resulting in a pixel size of ca. 375 nm and a field-of-view of ca. 750 μm. For each set of tomographic data, 501 radiographic projections were obtained at discrete angular steps with an exposure time of 100–120 s. The radiographic projections collected were reconstructed using a cone-beam filtered back projection algorithm (XMReconstructor, Zeiss) to produce a set of tomographic slices making up a cylindrical volume.

2.6. X-ray micro-tomography data processing

Tomographic images were imported into Avizo (Avizo 2022.1, Thermo Fisher Scientific) for processing and analysis. Sub-volumes were cropped for each tomogram with dimensions of 376 $\times$ 376 $\times$ 376 cubic voxels.

To assist with visualisation, a non-local means filter was applied to each tomographic image. Thresholding segmentation was conducted to identify each phase within the positive electrode material. A connected objects image was computed as a 16-bit file to isolate Li_2S and S images, with additional sieve analysis completed to exclude particles less than 4 cubic voxels (<1.50 μm particle size).

3. Results and discussion

3.1. ZELiS baseline cell development

Figure 1(a) illustrates the general design of the ZELiS cell, initially containing a Li_2S/carbon/binder-based positive electrode, a liquid electrolyte and metal CC. The as-received Li_2S powder was shown to be phase-pure by XRD (figure S1 in the supporting information (SI)). Slurry mixtures were prepared in accordance with the method outlined for ink and positive electrode preparation, with a general preparation schematic shown in figure 1(b). Handling Li_2S necessitates the use of an Ar-filled glovebox during all stages of preparation due to its reactivity upon air exposure. Therefore, toluene as the slurry solvent was preferred due to its high volatility, not requiring heat to be removed.

Porous 3D-carbon substrates have commonly been used as the positive electrode substrates to facilitate Li_2S activation and cycling. However, it is notable that when included in calculations of the inactive material in the positive electrode composite, this can comprise ∼50 to over 70 wt% [10, 15, 23, 32]. When preparing electrodes, the same carbon substrate was used and the overall carbon content was targeted to be ∼55 wt%.

Ball milling was used to reduce the particle size, improve the activation of Li_2S and make a uniform slurry. The slurry mixture and ball milling procedure were carried out in accordance with previous studies [23, 33, 34]. A loading of 2 mg cm^{-2}_{Li2S} was chosen for this work due to inconsistent and poor cell performance at higher loading values. With this fixed positive electrode fabrication procedure and a loading of 2 mg cm^{-2}_{Li2S}, a systematic study was carried out to understand the influence of different CC materials and electrolyte volume on the cell performance.

3.2. CC material

In ZEL cells, the choice of CC is an important parameter, as it is the surface on which the Li metal deposits. Three different metallic CCs were investigated based on their commercial availability and existing use in the battery industry: Cu, Ni and stainless steel. Both Cu and Ni have been adopted in previous studies [10, 11]. Foils were used as-received with no pre-cycle treatment.

Figure 2 displays the surface morphology of the 3 negative CCs. Generally, all the foils contain slightly pitted surfaces with minor scratches across them, likely ingrained from the manufacturing process [35]. The performance of these metals was tested over 50 cycles at a 1 C rate, shown in figure 2(d).

Cells using Ni and Cu CCs exhibited similar performance, while stainless steel showed a lower average capacity throughout all 50 cycles. However, the disassembly of multiple cells revealed a dark crusty build up on the Cu CC. In addition, optical microscopy images revealed a similar layer formation on the edge of the CC during the pre-cycle resting (figure S2). Over a short cycle-life period (<50 cycles) this does not appear to affect capacity retention. However, this is consistent with the reactivity of Cu with S species to form CuS over prolonged cycling. Due to the issue with long term cycling stability of Cu in LiS batteries [36], and the poor performance of the SS, the use of Ni was preferred.

3.3. Influence of electrolyte to active material ratio

The quantity of electrolyte used within LiS batteries has previously been shown to be a highly influential parameter on cycling performance. Figure 4 displays the electrochemical performance of five electrolyte to Li_2S mass loading ratios (E:S). This range was chosen to bridge the gap between commercialization targets and laboratory research. The exact E:S quantities are defined in table S1 in the SI.

Figure 3 shows that using higher quantities of electrolyte resulted in improved capacity retention. Cells containing 5 ml g^{-1}_{Li2S} performed worst, only achieving a capacity of 36 mAh g^{-1}_{Li2S} after 100 cycles. On the other hand, cells containing 15 and 20 ml g^{-1}_{Li2S} performed similarly well, suggesting >15 ml g^{-1}_{Li2S} of electrolyte is not needed. To balance cell performance while minimising electrolyte, an E:S ratio of 15 ml g^{-1}_{Li2S} was chosen. Due to the low electrolyte volumes, the electrolyte becomes quickly saturated with polysulfides which, as they undergo the shuttle effect, decrease the active utilisation of the active sulfur species. This is mainly through undergoing undesirable side reactions at the negative electrode associated with the electrolyte reacting with freshly deposited Li and the formation of inactive clusters of material within the electrolyte [14, 37].

After 100 cycles, the cells containing 15 and 20 ml g^{-1}_{Li2S} achieved 342 and 350 mAh g^{-1}_{Li2S}, respectively. These values are closely aligned with each other, whereas the cell containing 10 ml g^{-1}_{Li2S} shows a dramatic fall off to 221 mAh g^{-1} after 100 cycles. From these values, it can be deduced that using 15 ml g^{-1}_{Li2S}

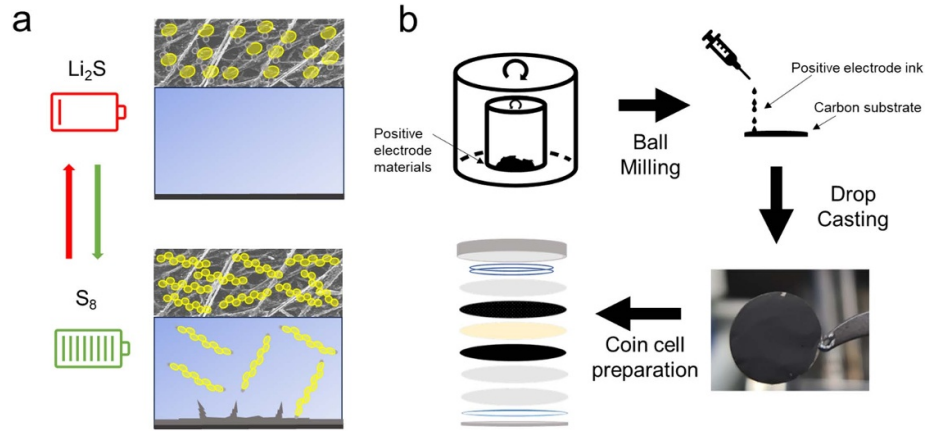

Figure 1. (a) Schematic of the ZELiS cell during operation. (b) Procedure for the preparation of Li_2S composite positive electrodes used in coin cells.

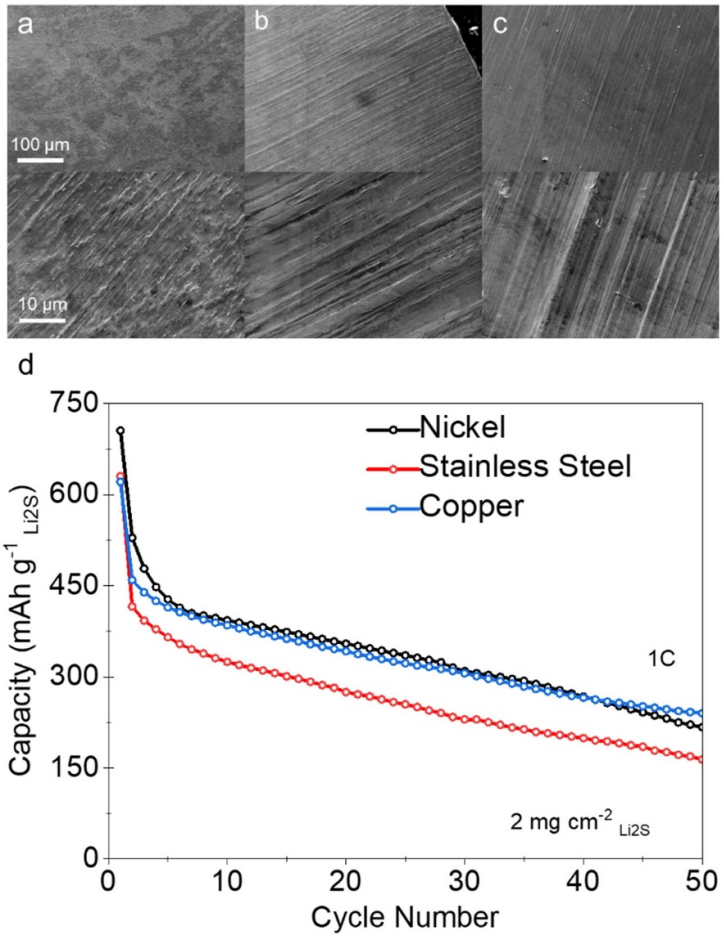

Figure 2. Scanning electron microscopy images of (a) Cu, (b) Ni and (c) stainless steel negative electrode current collector surfaces. (d) Electrochemical cycling data using three different metallic current collectors.

represents a critical point during cycling for capacity retention. Below this threshold, capacity fade is more significant with longer-term cycling, while above it, improvements in capacity gain are negligible.

Greater E:S ratios had a positive effect on the initial capacity achieved and the trend of capacity with cycle number. This is particularly pronounced in the initial 5 cycles, where cells featuring 5 and 7.5 ml g^{-1}_{Li2S} exhibited steep drops in capacity: falling to 25% and 62% of the initial capacities respectively, and considerably lower than the other E:S ratios. In general, excess electrolyte is beneficial for cell cycling [30, 38–41]. However, the performance of the battery containing 5 ml g^{-1}_{Li2S} is significantly lower than equivalent LiS cells previously reported but this has not previously been reported specifically for a ZELiS set

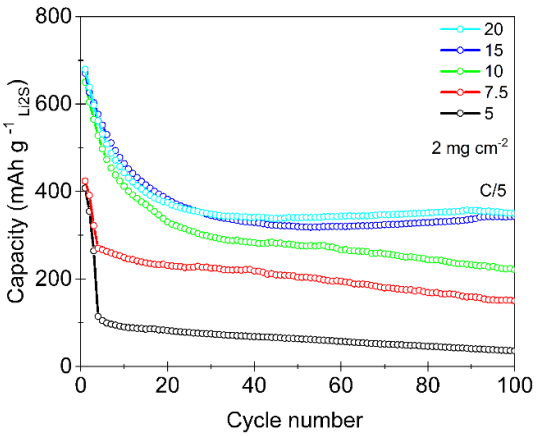

Figure 3. Cycling capacity per gram of Li_2S vs. cycle number for five different electrolyte-to-Li_2S mass loading ratios (E:S) in ml g^{-1}_{Li2S}.

up. This indicates the lower electrolyte volumes result in worse Li_2S activation. There are some key differences between these two cells, (i) the use of Li_2S, which is significantly less electrochemically active than Sulfur, (ii) the carbon matrix used as the positive electrode CC, which, due to being porous, prevents electrode wetting. The initial oxidation of Li_2S is intrinsically slow and proceeds via a solid-to-liquid phase reaction [24]. Vizintin *et al* showed at low E:S ratios, direct conversion of Li_2S to S_8 was preferred due to the formation of polysulfides being kinetically hindered [42]. Due to the porous carbon CC and subsequent poor wetting of the positive electrode, this results in particularly low initial oxidation of active Li_2S molecules in cycle one and subsequent cycles after.

Following this, the components and parameters of a baseline cell were established: a 2 mg cm^{-2} Li_2S positive electrode, a Ni-foil negative CC, and an electrolyte quantity of 15 ml g^{-1}_{Li2S}.

3.4. Formation cycle characterisation

Figure 4(a) shows a typical formation cycle of a ZELiS cell. The positive electrode begins as Li_2S with an initial voltage of 0.0 V. During charging, where Li_2S undergoes conversion to S_8, the voltage rapidly increased to a 3.0 V plateau for the majority of the first charge, before rapidly increasing again up to the 4.0 V cut-off. This minimised any oxidation of the electrolyte and was considered a trade-off to utilising all the active material in the positive electrode. In addition, due to the large excess of electrolyte adopted in the cell, the losses of electrolyte from oxidation at this voltage were considered negligible [10, 11, 25, 39, 43]. On discharge, a double plateau was observed, indicating the conventional Li-S multi-stage reduction mechanism, where the mixed product Li_2S/Li_2S_2 has been reported [44, 45].

Whilst the formation process is well documented for LiS positive electrodes [40], detailed studies in a ZELiS set-up are lacking. Specifically, very little is known about the state of the active materials within the carbon CC. To investigate these properties, micro-CT images of different ZELiS positive electrodes were scanned *ex-situ* at different states of charge (figures 4(b)–(d)).

Li_2S particles with an average diameter ($\varnothing_{ave}$) of 1.54 μm were observed in the pristine electrode (figure 4(b)). The small particle size was consistent with a low overpotential for Li_2S conversion (charge voltage plateau at ~3.0 V (figure 4(a))), which has been observed for ball-milled Li_2S [33, 34]. Good distribution throughout the electrode was seen, which is thought to be also desirable for facile Li_2S activation [23]. Figure 4(c) shows the positive electrode in the charged state. The morphology of the S_8 differs significantly from the Li_2S particles, showing some agglomeration and less well dispersed particles generally. The S_8 average particle size was 4.11 μm, significantly bigger than the pristine Li_2S particles. At the end of discharge (figure 4(d)), the Li_2S/Li_2S_2 products reformed with similar dispersion to the pristine, however their average diameter increased to 2.90 μm.

The changes in particle size and morphology are likely a consequence of S/Li_2S particles re-depositing away from their original location during formation. The underlying mechanisms are complex and not well understood. One candidate is electrolyte 'sink', a phenomenon first reported Zielke *et al* [46], and subsequently by Yermukhambetova *et al* [47], where S species precipitate from the electrolyte deep back into the 3D carbon matrix and become less accessible for subsequent cycles leading to a loss of active material and capacity. Additionally, the dissimilar rates at which polysulfides transport in and out of the positive electrode may result in concentration gradients. Studies by Lin *et al*, and Xu *et al*, found this to be influential on S

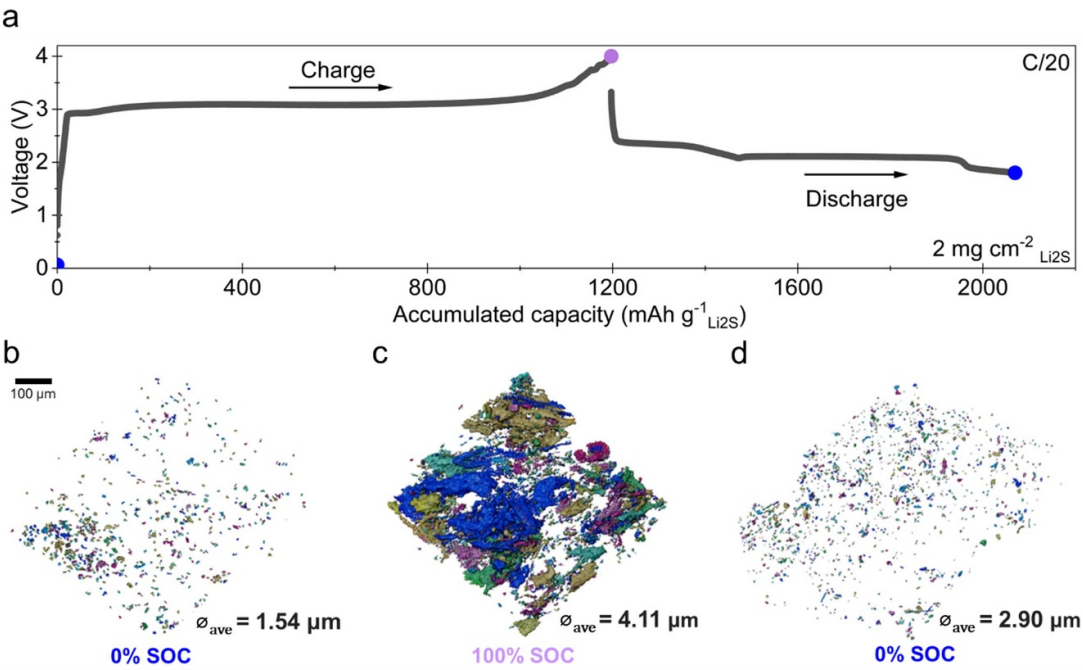

Figure 4. (a) Formation cycle of a ZELiS battery. Volume rendering images at 20× magnification of *ex-situ* Li_2S positive electrode substrates at different states of charge during a formation cycle: (b) Pristine state (Li_2S), (c) charged state (S_8) and (d) discharged state (Li_2S/Li_2S_2). Scale bar is 100 μm for all three images; $\varnothing_{ave}$ denotes average particle diameter.

particle morphology and size in LiS cells [44, 45]. Both mechanisms support the observation of increasing particle sizes during the initial cycle(s) leading to permanent degradation and loss of active material.

Figure 5 displays the cell impedance at difference points in the formation cycle. Li-S cells are known to exhibit numerous (>5) overlapping polarisation processes, requiring advanced analytical techniques, such as distribution of relaxation times analysis [48, 49], to deconvolute them. As this is not the focus of our study, here we will qualitatively analyse the EIS of ZELiS cells. Initially, the pristine cell (Li_2S positive electrode|bare CC) exhibits one, possibly two, semi-circle(s) indicating charge transfer processes followed by a very steep tail in the low frequency region, i.e., the expected blocking electrode behaviour. After the first charge, where a Li electrode has been electrochemically deposited, a low frequency tail with two depressed semi-circles at high frequency were clearly observed. These may indicate several overlapping polarisation processes. Additionally, the real axis intercept shifted to higher impedance values, likely due to the presence of polysulfides in the electrolyte. Following discharge, depressed semi-circles were observed again but without blocking electrode behaviour. Based on these impedance datasets, the cell does not return to its original state after formation due to the different electrolyte composition and residual Li on the CC [29].

3.5. Effect of C-rate on cycling performance

To replace current state-of-the-art Li-ion batteries, devices capable of operating consistently at high-power density is an important parameter. The effect of C-rate on the optimised ZELiS cell architecture is depicted in figure 6. Note the good reproducibility over 12 devices ($N = 4$ for each rate). The highest capacity retention was seen at low C-rates, where 270 mAh g^{-1}_{Li2S} was achieved after 200 cycles at C/10, vs. 110 mAh g^{-1}_{Li2S} at 1C. Similarily, the lowest C-rate achieved the highest CE, 99.36% over 200 cycles at C/10 vs 98.65% at 1C.

All cells exhibited a large drop in capacity within the first five cycles. This was most severe at 1C, equivalent to a 50% capacity loss in cycle 1. At slower rates, the capacity decay was still significant but lessened: declining 26% and 31% in cycle 1 for C/5 and C/10 respectively. The CE values for cycle 1 were also low, before stabilising at 98%–100% for the remaining cycles for all 3 C-rates In the case of C/5 and C/10, a small increase in capacity followed by a plateau was observed around 100 cycles (figure 6), before a consistent decline towards cycle number 200.

The initial drop in capacity has been attributed to degradation of the *in-situ* Li negative electrode with contributions from sulfur inventory losses [32]. The difference in cell capacities between the different C-rates is likely a consequence of kinetic limitations and increased resistance often observed at higher rates [38], while the capacity increase observed around 100 cycles may be due to polysulfide reabsorption into the positive electrode [13]. This would indicate that the conversion back to Li_2S/Li_2S_2 on discharge is significantly lower than the reverse process on charge, leading to a steadily increasing concentration of

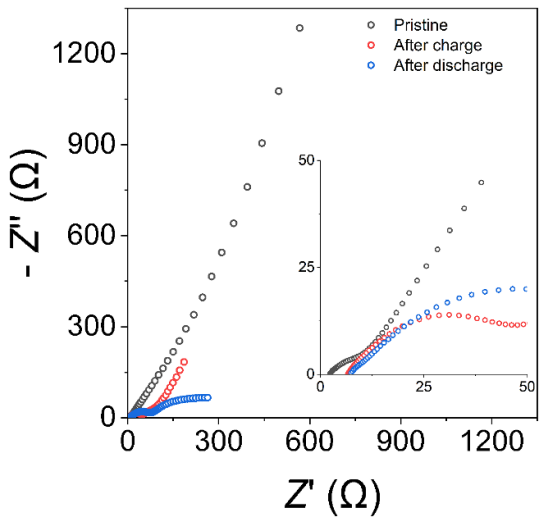

Figure 5. Electrochemical impedance spectroscopy of a ZELiS cell formation cycle, with a zoomed inset. Frequency range from 1 MHz to 0.1 Hz.

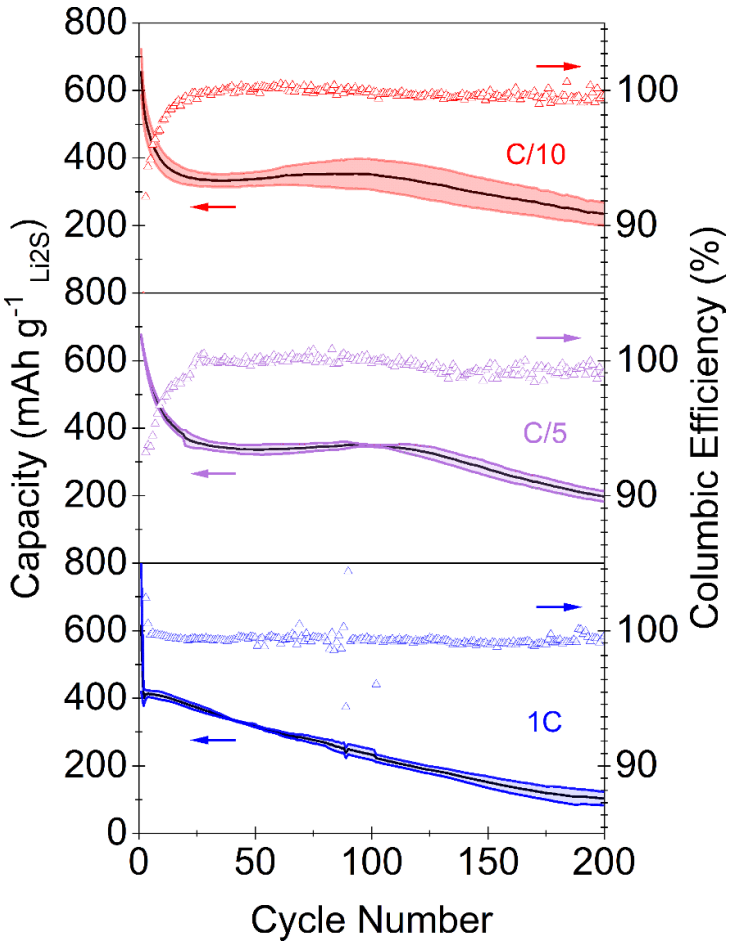

Figure 6. Mean discharge capacity over 200 cycles of several ZELiS cells at C/10, C/5 and 1 C rates. The number of repetitions for all C-rates was $N = 4$ and the shaded area in each indicates ± 1 standard deviation. Cells were composed of a 2 mg $cm^{-2}{}_{Li2S}$ positive electrode, Ni current collector and an E:S ratio of 15 ml $g^{-1}{}_{Li2S}$.

polysulfides in the electrolyte. A dynamic equilibrium between the redox species could allow more active material to slowly become more accessible at later cycles [22]. This is followed by sustained irreversible losses from both electrodes leading to capacity values of ∼200 mAh $g^{-1}{}_{Li2S}$ for both C/5 and C/10 rates after 200

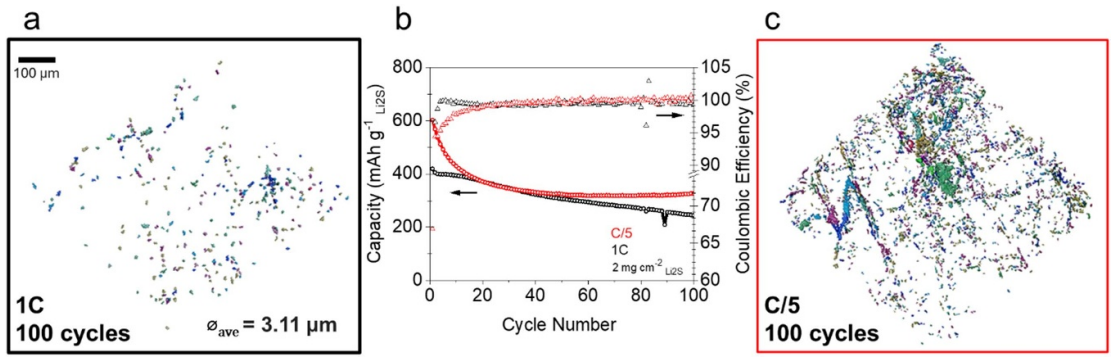

Figure 7. Volume rendering images of *ex-situ* positive electrode substrates after 100 cycles at (a) 1C (c) C/5 rates. The corresponding electrochemical cycling data for each C-rate is shown in (b). Cells were composed of a 2 mg cm$^{-2}_{Li2S}$ positive electrode, Ni current collector and an E:S ratio of 15 ml g$^{-1}_{Li2S}$. (scale bar is 100 μm for all three images, ø$_{ave}$ denotes average particle diameter).

cycles. The difference between 1C and the slower C-rates was stark, therefore to better understand the underlying processes, x-ray micro-CT imaging was performed.

Figures 7(a) and (c) displays CT images of positive electrodes following 100 cycles (figure 7(b)) at different (dis)charging rates. At the higher C-rate, there appeared to be substantially fewer Li_2S/S particles and less particle agglomeration. The average particle size was smaller for the 1 C rate: 3.11 μm compared to 3.88 μm for C/5. This would indicate the polysulfide shuttle effect is stronger at high C-rates, causing more permanent loss of S species, leaving fewer, smaller particles within the electrode available to react, and vice versa. Studies of conventional Li-S cells have shown a similar C-rate-capacity correlation and found the degradation mechanism may show a time dependency [38].

3.6. Recommendations

With the considerations above, this leads to the following recommendations to continue improving and maximising the potential of ZELiS cells and general 'anode-free' cell research. First, whilst slurry mixtures often contain low quantities of carbon (<30 wt%), the actual inactive material value can be significantly higher (>70 wt%) due to the commonly used carbon paper substrate. Next phases of research should aim to reduce this (or remove entirely), by moving to metallic foils for example, to improve energy density metrics. The use of metallic meshes as substrates can be used to improve the efficiency and C-rate performance of the cell. However, these also add additional weight, in addition to posing significant manufacturing challenges. Secondly, the electrolyte is an important component of the Li-S chemistry, however, it also contributes the largest weight fraction to the specific energy of a ZELiS cell. Therefore, future work should aim to reduce this to less than 5 ml g$^{-1}_{Li2S}$. Achieving this is challenging, due to the poor activation of Li_2S at low electrolyte volume and rapid performance decline as electrolyte volume decreases (figure 3). Electrolytes must be designed to be highly soluble for redox active lithium-polysulfides, ionically conductive and minimize polysulfide shuttling. One approach is to minimise polysulfide shuttling by using weakly solvating solvents, however this can restrict access to the active sulfur material leading to poorer cycling. Instead, this has mainly been achieved by highly concentrated ether-based electrolytes with Li-salts, however other electrolyte systems, including solid state electrolytes, highly concentrated salts, dual-salts and functional additives [1, 50]. In particular, highly-concentrated electrolyte systems should be prioritised due to their recent resurgence and potential promise of high energy Li-S batteries [19, 20].

4. Conclusions

In summary, we report a consistent ZELiS cell comprising a Ni negative CC, E:S ratio of 15 ml g$^{-1}_{Li2S}$ and active material loading of 2 mg cm$^{-2}_{Li2S}$ in a carbon paper substrate. This configuration achieved ~270 mAh g$^{-1}_{Li2S}$ after 200 cycles at C/10 rate. All cells exhibited substantial capacity decline within the first 5 cycles, experiencing greater losses at higher C-rates. However, at C/5 and C/10 the initial drop was less steep and a small increase in capacity was observed around 100 cycles, suggesting time-dependent dynamics of sulfur conversion. X-ray micro-CT imaging showed that significantly more active material was retained at a C/5 rate vs. 1C. We hope that this study provides a robust and 'fail fast' platform for future investigations on electrode and electrolyte modifications. Strategies aimed at reducing conductive additive content,

minimising and refining the electrolyte, and optimizing the management of sulfur species in redox reactions will be pivotal in realising the promise of ZELiS cells.

Data availability statement

The data cannot be made publicly available upon publication because the cost of preparing, depositing and hosting the data would be prohibitive within the terms of this research project. The data that support the findings of this study are available upon reasonable request from the authors.

Acknowledgment

The authors acknowledge the support of The Faraday Institution's LiSTAR Programme (FIRG061). PRS was supported by the Department of Science, Innovation and Technology (DSIT) and the Royal Academy of Engineering under the Chair in Emerging Technologies programme (CiET1718/59).

ORCID iDs

Joshua H Cruddos https://orcid.org/0000-0002-0757-8337
James B Robinson https://orcid.org/0000-0002-6509-7769
Paul R Shearing https://orcid.org/0000-0002-1387-9531
Alexander J E Rettie https://orcid.org/0000-0002-2482-9732

References

[1] Bhargav A, He J, Gupta A and Manthiram A 2020 Lithium-sulfur batteries: attaining the critical metrics *Joule* **4** 285–91
[2] Manthiram A, Fu Y, Chung S H, Zu C and Su Y S 2014 Rechargeable lithium-sulfur batteries *Chem. Rev.* **114** 11751–87
[3] Chung S H, Chang C H and Manthiram A 2018 Progress on the critical parameters for lithium–sulfur batteries to be practically viable *Adv. Funct. Mater.* **28** 1801188
[4] Xue W, Miao L, Qie L, Wang C, Li S, Wang J and Li J 2017 Gravimetric and volumetric energy densities of lithium-sulfur batteries *Curr. Opin. Electrochem.* **6** 92–99
[5] Pathak A D, Cha E and Choi W 2024 Towards the commercialization of Li-S battery: from lab to industry *Energy Storage Mater.* **72** 103711
[6] Chung S H and Manthiram A 2018 Designing lithium-sulfur cells with practically necessary parameters *Joule* **2** 710–24
[7] Zhu K, Wang C, Chi Z, Ke F, Yang Y, Wang A, Wang W and Miao L 2019 How far away are lithium-sulfur batteries from commercialization? *Front. Energy Res.* **7** 1–12
[8] Wang M, Bai Z, Yang T, Nie C, Xu X, Wang Y, Yang J, Dou S and Wang N 2022 Advances in high sulfur loading cathodes for practical lithium-sulfur batteries *Adv. Energy Mater.* **12** 2201585
[9] Liu H, Lai W H, Yang Q, Lei Y, Wu C, Wang N, Wang Y X, Chou S L, Liu H K and Dou S X 2021 Understanding sulfur redox mechanisms in different electrolytes for Room-temperature Na–S batteries *Nano-Micro Lett.* **13** 1–14
[10] Nanda S, Bhargav A and Manthiram A 2020 Anode-free, lean-electrolyte lithium-sulfur batteries enabled by tellurium-stabilized lithium deposition *Joule* **4** 1121–35
[11] Nanda S, Gupta A and Manthiram A 2018 A lithium–sulfur cell based on reversible lithium deposition from a Li_2S Cathode Host onto a Hostless-anode substrate *Adv. Energy Mater.* **8** 2–7
[12] Robinson J B, Xi K and Kumar R V 2021 2021 roadmap on lithium sulfur batteries *J. Phys.* **3** 031501
[13] Li G, Wang X, Seo M H and Prum R O 2018 Chemisorption of polysulfides through redox reactions with organic molecules for lithium–sulfur batteries *Nat. Commun.* **9** 1–10
[14] Deng C, Wang Z, Wang S and Yu J 2019 Inhibition of polysulfide diffusion in lithium-sulfur batteries: mechanism and improvement strategies *J. Mater. Chem.* A **7** 12381–413
[15] Nanda S, Gupta A and Manthiram A 2021 Anode-free full cells: a pathway to High-energy density lithium-metal batteries *Adv. Energy Mater.* **11** 1–18
[16] Yu X and Manthiram A 2018 Electrode-electrolyte interfaces in lithium-based batteries *Energy Environ. Sci.* **11** 527–43
[17] Ding N, Zhou L, Zhou C, Landi S, Tonazzini I, Cecchini M, Piazza V and Gemmi M 2016 Building better lithium-sulfur batteries: from $LiNO_2$ to solid oxide catalyst *Sci. Rep.* **6** 1–10
[18] Cheng X B and Zhang Q 2015 Dendrite-free lithium metal anodes: stable solid electrolyte interphases for high-efficiency batteries *J. Mater. Chem.* A **3** 7207–9
[19] Liu J, Li S, Nomura N, Ueno K, Dokko K and Watanabe M 2024 Enhancing Li-S battery performance with limiting Li[N(SO2F)2] content in a sulfolane-based sparingly solvating electrolyte *ACS Appl. Mater. Interfaces* **16** 8570–9
[20] Castillo J *et al* 2024 Graphene-based sulfur cathodes and dual salt-based sparingly solvating electrolytes: a perfect marriage for high performing, safe, and long cycle life lithium-sulfur prototype batteries *Adv. Energy Mater.* **14** 2023023781
[21] Zhao M, Li B Q, Zhang X Q, Huang J Q and Zhang Q 2020 A Perspective toward practical lithium-sulfur batteries *ACS Cent. Sci.* **6** 1095–104
[22] Wild M, O'Neill L, Zhang T, Purkayastha R, Minton G, Marinescu M and Offer G J 2015 Lithium sulfur batteries, a mechanistic review *Energy Environ. Sci.* **8** 3477–94
[23] Yang Y, Zheng G, Misra S, Nelson J, Toney M F and Cui Y 2012 High-capacity micrometer-sized Li_2S particles as cathode materials for advanced rechargeable lithium-ion batteries *J. Am. Chem. Soc.* **134** 15387–94
[24] Ye H, Li M, Liu T, Li Y and Lu J 2020 Activating Li_2S as the lithium-containing cathode in lithium-sulfur batteries *ACS Energy Lett.* **5** 2234–45

[25] Chen J, Xiang J, Chen X, Yuan L, Li Z and Huang Y 2020 Li2S-based anode-free full batteries with modified Cu current collector *Energy Storage Mater.* **30** 179–86
[26] Zhang C, Lan Q, Liu Y, Wu J, Shao H, Zhan H and Yang Y 2019 A dual-layered artificial solid electrolyte interphase formed by controlled electrochemical reduction of LiTFSI/DME-LiNO3 for dendrite-free lithium metal anode *Electrochim. Acta* **306** 407–19
[27] Weber R, Genovese M, Louli A J, Hames S, Martin C, Hill I G and Dahn J R 2019 Long cycle life and dendrite-free lithium morphology in anode-free lithium pouch cells enabled by a dual-salt liquid electrolyte *Nat. Energy* **4** 683–9
[28] LiSTAR *Lithium-Sulfur Technology Accelerator* (available at: www.listar.ac.uk/) (Accessed 14 January 2025)
[29] Soni R, Robinson J B, Shearing P R, Brett D J L, Rettie A J E and Miller T S 2022 Lithium-sulfur battery diagnostics through distribution of relaxation times analysis *Energy Storage Mater.* **51** 97–101
[30] Agostini M, Hwang J-Y, Kim H M, Bruni P, Brutti S, Croce F, Matic A and Sun Y-K 2018 Minimizing the electrolyte volume in Li–S batteries: a step forward to high gravimetric energy density *Adv. Energy Mater.* **8** 1801560
[31] Vadhva P, Hu J, Johnson M J, Stocker R, Braglia M, Brett D J L and Rettie A J E 2021 Electrochemical impedance spectroscopy for all-solid-state batteries: theory, methods and future outlook *ChemElectroChem* **8** 1930–47
[32] Nanda S and Manthiram A 2020 Lithium degradation in lithium-sulfur batteries: insights into inventory depletion and interphasial evolution with cycling *Energy Environ. Sci.* **13** 2501–14
[33] Cai K, Song M K, Cairns E J and Zhang Y 2012 Nanostructured Li_2S-C composites as cathode material for high-energy lithium/sulfur batteries *Nano Lett.* **12** 6474–9
[34] Ting L K J, Gao Y, Wang H, Wang T, Sun J and Wang J 2022 Lithium sulfide batteries: addressing the kinetic barriers and high first charge overpotential *ACS Omega* **7** 40682–700
[35] Sabi N, Palanisamy K, Rahide F, Daboss S, Kranz C and Dsoke S 2023 Surface properties-performance relationship of aluminum foil as negative electrode for rechargeable aluminum batteries *Batter Supercaps* **6** 1–14
[36] Robba A, Mežnar M, Vizintin A, Bitenc J, Bobnar J, Arčon I, Randon-Vitanova A and Dominko R 2020 Role of Cu current collector on electrochemical mechanism of Mg–S battery *J. Power Sources* **450** 227672
[37] Coke K, Johnson M J, Robinson J B, Rettie A J E, Miller T S and Shearing P R 2023 Illuminating polysulfide distribution in lithium sulfur batteries; tracking polysulfide shuttle using operando optical fluorescence microscopy *ACS Appl. Mater. Interfaces* **16** 20329–40
[38] Brückner J, Thieme S, Grossmann H T, Dörfler S, Althues H and Kaskel S 2014 Lithium–sulfur batteries: influence of C-rate, amount of electrolyte and sulfur loading on cycle performance *J. Power Sources* **268** 82–87
[39] Yen Y J and Manthiram A 2024 Anode-free lithium-sulfur batteries with a rare-earth triflate as a dual-function electrolyte additive *ACS Appl. Mater. Interfaces* **16** 34997–5005
[40] Li G, Wang S, Zhang Y, Li M, Chen Z and Lu J 2018 Revisiting the role of polysulfides in lithium–sulfur batteries *Adv. Mater.* **30** 1705590
[41] Zhang K, Lee G H, Park M, Li W and Kang Y M 2016 Recent developments of the lithium metal anode for rechargeable non-aqueous batteries *Adv. Energy Mater.* **6** 1600811
[42] Vizintin A, Chabanne L, Tchernychova E, Arčon I, Stievano L, Aquilanti G, Antonietti M, Fellinger T P and Dominko R 2017 The mechanism of Li_2S activation in lithium-sulfur batteries: can we avoid the polysulfide formation? *J. Power Sources* **344** 208–17
[43] Lai T, Bhargav A and Manthiram A 2023 Lithium tritelluride as an electrolyte additive for stabilizing lithium deposition and enhancing sulfur utilization in anode-free lithium–sulfur batteries *Adv. Funct. Mater.* **33** 2304568
[44] Xu R *et al* 2014 Insight into sulfur reactions in Li-S batteries *ACS Appl. Mater. Interfaces* **6** 21938–45
[45] Lin C N, Chen W C, Song Y F, Wang C C, Tsai L D and Wu N L 2014 Understanding dynamics of polysulfide dissolution and re-deposition in working lithium–sulfur battery by in-operando transmission x-ray microscopy *J. Power Sources* **263** 98–103
[46] Zielke L *et al* 2015 Degradation of Li/S battery electrodes on 3D current collectors studied using x-ray phase contrast tomography *Sci. Rep.* **5** 1–12
[47] Yermukhambetova A, Tan C, Daemi S R, Bakenov Z, Darr J A, Brett D J L and Shearing P R 2016 Exploring 3D microstructural evolution in Li-Sulfur battery electrodes using *in-situ* x-ray tomography *Sci. Rep.* **6** 1–9
[48] Qiu X, Hua Q, Zheng L and Dai Z 2020 Study of the discharge/charge process of lithium-sulfur batteries by electrochemical impedance spectroscopy *RSC Adv.* **10** 5283–93
[49] Gerle M, Wagner N, Häcker J, Nojabaee M and Friedrich K A 2022 Identification of the underlying processes in impedance response of sulfur/carbon composite cathodes at different SOC *J. Electrochem. Soc.* **169** 030505
[50] Gupta A, Bhargav A and Manthiram A 2019 Highly solvating electrolytes for lithium–sulfur batteries *Adv. Energy Mater.* **9** 1803096